Flexible MXene/EPDM rubber with excellent thermal conductivity and electromagnetic interference performance

Shaowei Lu[1] · Bohan Li[1] · Keming Ma[1] · Sai Wang[1] · Xingmin Liu[1] · Ziang Ma[1] · Lunyang Lin[2] · Guannan Zhou[2] · Dongxu Zhang[2]

Abstract

In this study, a rubber composite was prepared based on two-dimensional (2D) material (MXene) and ethylene propylene diene rubber (EPDM). The MXene was efficiently prepared by etching Ti_3AlC_2 powder with LiF-HCl solution and subsequent vacuum drying, and the dispersion of MXene in EPDM was improved by optimizing the grinding process, ultrasonic stripping and stirring method. In the process of exploring the electrical conductivity of this material system, the composite exhibits low percolation threshold of 2.7 wt%, a high conductivity of 106 Sm^{-1} and superior thermal conductivity of 1.57 W/m K at the MXene content of 6 wt%. In addition, MXene (6 wt%)/EPDM with 0.3-mm thick exhibits an EMI shielding performances (SE) up to 48 dB in the X-band (8.2–12.4 GHz) and 52 dB in the Ku-band (12.4–18 GHz) (SE) which are much better than the electromagnetic shielding properties of other rubber blends, and these properties indicate MXene/EPDM composite has great potential for versatile applications.

Keywords Two-dimensional materials (MXene)/EPDM · Percolation threshold · Thermal conductivity · Electromagnetic interference shielding

1 Introduction

With the rapid development of modern electronic industry, electronic appliances and wireless communication are widely used, and electromagnetic interference (EMI) has become an urgent problem need to be solved in electronic industry and daily life [1–3], at the same time, a lot of heat is generated by some electronics, which can harm the performance and lifetime of these source electronics and other nearby electronics [4]. Therefore, EMI shielding and thermal dispersion are indispensable in the design and application of electronic devices, and excellent flexible materials for electromagnetic shielding and thermal dispersion are imminently desired.

Metals and alloys, the most commonly used for EMI shielding material, not only have excellent conductivity, but also have the function of absorbing and reflecting electromagnetic interference [5]. However, the large density, poor flexibility and limited thermal conductivity limit their range of application and effect of use [6]. In order to solve these problems, various alternative nanomaterials are used to design EMI materials, such as carbon nanotubes (CNTs)-based composites [7, 8] and graphene-based composites [9]. The EMI shielding materials are designed reasonably by CNTs, but in general, the EMI shielding of CNTs-based composites is about 23.8 dB (poly(ε-caprolactone)/multiwall carbon nanotube) [8], 26–73 dB (30 wt% MWCNT/silicone) [10], and the EMI performances may be different from the expected since it is not possible to avoid entangled aggregates due to a non-uniform dispersion of the fillers within base material which affects the mechanical and the electrical response of the obtained nanocomposites. Similarly, for the graphene blend EMI shielding materials, although its conductivity is larger than that of carbon nanotubes, its dispersion is a hard nut to crack, which leads to unsatisfactory EMI shielding of 5 wt% graphene/cyanateester (38 dB) [11], 8 wt% GnPs/EPDM(33 dB) [12] and 10% graphene

✉ Shaowei Lu
  lushaowei_2005@163.com

[1] Faculty of Materials Science and Engineering, Shenyang Aerospace University (SAU), Shenyang 110136, China

[2] Faculty of Aeronautical and Astronautical Engineering, Shenyang Aerospace University (SAU), Shenyang 110136, China

enhanced flexible expanded graphite film (48.3 dB) [13] In view of the influence of difficult dispersion of carbon nanotubes and graphene on EMI shielding properties, it is necessary to find a high-performance EMI nanomaterial which is easy to disperse.

Two-dimensional (2D) materials have attracted wide attention due to their excellent properties (electronic, thermal, electromagnetic, etc.) [14–17], the 2D transition metal carbides or nitrides called MXenes [18, 19], MXene phases that generally conforms to the formula of M_nAX_{n-1}, where "M" usually represents early transition metal (Ti, Mo, V, etc.), "A" is aluminum (Al), silicon (Si) or other groups of IIIA or IVA element [20]. X is carbon or nitrogen [21, 22]. Up to now, MXene series includes Ti_3C_2, Ti_2C, $(Ti_{0.5}, Nb_{0.5})_2C$, $(V_{0.5}, Cr_{0.5})_3C_2$, Ti_3CN, Ta_4C_3 [23], Nb_2C, V_2C [24] and Nb_4C_3 [25]. What's worth mentioning is that the outstanding hydrophilicity and lipophilicity of MXenes make them attractive as fillers in many polymers. The MXenes also show distinguished conductivities, for instance, the conductivity of pure MXene films is as high as 2.4×10^5 S/m which is much higher than the graphene (about 6000 s/cm [26]) and the carbon nanotube (about 200 s/cm). Besides, MXene shows the excellent electromagnetic shielding performance, the shielding performance of MXene films up to 92 dB [27] higher than graphene (52.2 dB) [28]. The hydrophilicity/lipophilicity, conductivity, makes the MXene-based composites to be a promising EMI material in the field of nanomaterial–polymer composites.

It is also a typical unsaturated polyolefin rubber which is mainly used in tires, cables, gaskets, footwear, sporting goods and waterproof sheets for construction [29]. Unfortunately, EPDM cannot shield against electromagnetic radiations. Therefore, it is of great significance to use MXene to enhance the EMI performance of EPDM. Herein, we used simple and efficient methods to prepare MXene/EPDM nanocomposites. The dispersion of MXene in rubber matrix was increased by grinding and optimizing ultrasonic time, and the size of MXene film and the dispersion spacing in toluene were controlled. Thermal conductivity and electromagnetic shielding were explored by comparing MXene/EPDM rubber with different contents, and their mechanism was analyzed.

2 Experimental

2.1 Materials

The ethylene propylene diene monomer rubber (EPDM) with a density 0.78 g/cm³ was supplied by Shenyang aircraft company, Liaoning Province, China. Titanium aluminum carbide (Ti_3AlC_2) was supplied by Fosman Technology Co, Ltd, Beijing China. Lithium fluoride was purchased from

Panjin (China) Research Front Technology Co, Ltd. Concentrated hydrochloric acid (12 mol/L) was provided by Sinopharm Chemical Reagent Co., Ltd, Liaoning Province, China.

2.2 Sample preparation

2.2.1 Preparation of two-dimensional (2D) materials (MXene)

The MXene was synthesized according to a brief "corrosion–stripping" procedure. The bulk MXene precursor was slowly dispersed into HCl (9 mol/L)-LiF, and the dispersion was stirred with magnetic agitator for 24 h, after which the suspension product was washed repeatedly with deionized water until the supernatant reached to pH of 6.0, and the obtained suspension product was vacuum-dried at 80 °C for 12 h.

2.2.2 Fabrication of MXene/EPDM nanocomposites

We adopted a simple and efficient method to prepare MXene/EPDM, and the scheme is shown in Fig. 1. The EPDM rubber was put into a two-roller roll at room temperature for 1 h to add vulcanization agent, and the rubber was dissolved in toluene(48 h). We dispersed MXene in toluene solution by ultrasound (90 min) and blended dispersion with EPDM emulsion by the ultrasound method (2 h) and stirred for 5 h at 200 rpm. The mixture was poured into the mold and heated for 2 h at 80 °C in vacuum, and the MXene/EPDM composite was stripped from the mold. The curing conditions were heated at 170 °C for 30 min at 10 MPa pressure.

2.3 Characterization

The structural morphology of MXene/EPDM composites was characterized by scanning microscopy (SEM; Zeiss supra55). Fourier transform infrared spectroscopy (FTIR, Spectrum 100 spectrometer Perkin Elmer, USA) and Raman spectra (Thermofisher DXR Raman microscope, Thermo Scientific, USA) were used to test MXene lamellar. The electrical conductivity of different contents of MXene/EPDM composites was measured by a stand four-probe device (RTS-8, 4 PROBES TECH Co., Ltd., China). The thermal conductivity was examined by using the TC3000 (Q800, TA instrument, USA).

These tests included: (1) The optimal dispersion concentration and ultrasonic dispersion time of MXene were determined. (2) In order to improve the service performance, the conductivity of MXene/EPDM composites was measured from 1 to 6 wt%, and the permeation threshold was found. (3) The thermal conductivity of MXene/EPDM composites with different content is different at room temperature. (3)

Fig. 1 Schematic illustration of the fabrication process of MXene/EPDM composites
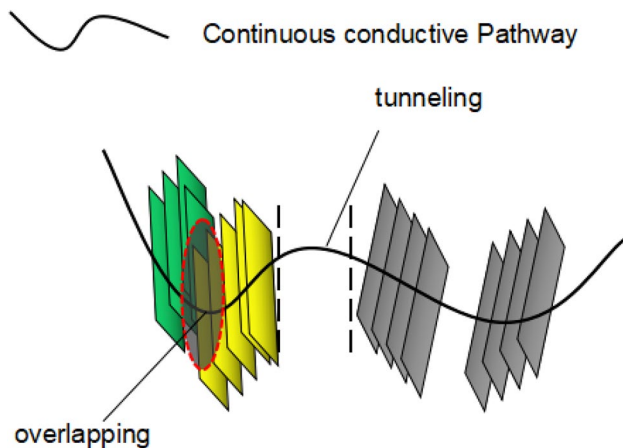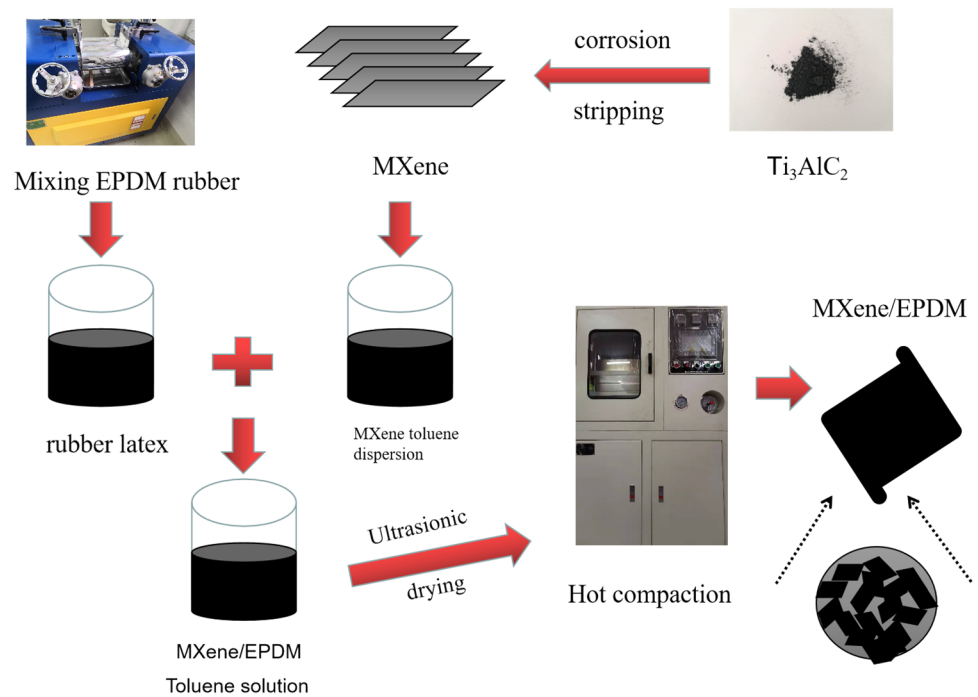

Fig. 2 Modeling of distribution of MXene platelets in EPDM

Test the shielding effectiveness of MXene/EPDM in X-band (8.2-12.4 GHz) and Ku-band (12.4-18 GHz).

2.4 Analytical model

The MXene resistance source connection network mainly composed of two parts: the inherent resistance of MXene and the resistance of MXene connection. MXene has two types of junctions: (1) full contact with overlap and (2) tunnel junctions over a certain distance, as shown in Fig. 2. It is believed that the relative contribution of the inherent piezoelectric behavior and discrete damage accumulation is considered significant before the penetration threshold. With the increase in MXene content, the conductive network gradually formed. After the percolation threshold, MXene is connected to each other by overlapping or/and tunnel connection, and the change of the connection distances will result a change in potential, and it makes the current carrier transmission unstable and produces the change of resistivity [30].

2.4.1 EMI shielding performance

The electromagnetic shielding performance of nanocomposite film is tested by a two-port vector network analyzer (PAN-LN5230L Agilent Technologies) using the waveguide method in X-band (8.2–12.4 GHz) and Ku-band (12.4–18 GHz). The size of the sample is 22.86×10.16 mm for X-band and 15.79×7.89 mm for Ku-band. The total shielding effectiveness (SET), shielding effectiveness absorption (SEA) and shielding effectiveness reflection (SER) are determined by the following formula according to the measured parameters.

$$R = |S11|^2 \quad T = |S21|^2 \tag{1}$$

$$A = 1 - R - T \tag{2}$$

$$SER(dB) = -10\log(1 - R) \quad SEA(dB) = -10\log(T/(1 - R)) \tag{3}$$

$$SET(dB) = 10\log\left(\frac{PI}{PT}\right) = SER + SEA \tag{4}$$

where R is the reflection coefficient and T is the absorption coefficient. P_I is the incident power, and P_T is the transmission power.

3 Results and discussion

3.1 Characterization of MXene/EDPM mixture

MXene dispersions are obtained from peeling MXene raw materials which etched and peeled by HCL-LiF fine as shown in Fig. 3a. It can be seen that the MXene dispersions in the water exhibit obvious Tyndall effect, which indicates that MXene has good dispersion. Figure 3b shows that the MXene powder has a small particle size. The MXene powder is dispersed in the rubber matrix and molded at 170 °C and 10 Mpa pressure for 30 min to obtain MXene/EPDM composite material as shown in Fig. 3c and d. The obtained MXene/EDPM rubber sheet with a smooth surface, uniform thickness of 0.3 mm and good flexibility allows MXene/EPDM to act as commercial portable flexible electrons.

In order to understand the effect of MXene on the electrical properties and thermal dispersion properties of MXene/EPDM composites, it is necessary to study their morphology. The morphology of MXene and MXene/EPDM composites was characterized respectively by SEM. As shown in Fig. 4a and b, the typical stripping 2D morphology of $Ti_3C_2T_x$ with different directions was observed, and MXene powder has an obvious accordion structure and the layer spacing of about 500 nm. The folded surface can promote the dispersion of MXene in EPDM matrix and improve the permeability level. At the same time, these nanosheets with many wrinkles and ripples are important to induce the attenuation of electromagnetic waves, because the structure can act as attentive centers of electromagnetic waves and electric trap centers, leading to dielectric losses [31–33]. As we can see in Fig. 4c and d, the MXene nanosheets still have a complete structure about 2 microns after ultrasound and evenly dispersed in the rubber matrix. And some MXene will connect together to form conductive network, and these interconnected MXene nanosheets network also can establish electrical and thermal conduction pathways in the whole MXene/EPDM nanocomposites, which is responsible for improving the conductivity and thermal conductivity of MXene/EPDM nanocomposites.

As shown in Fig. 5a, the surface state of layered MXene films was observed by FTIR. In Fig. 5a, the absorption bands at 3857, 3754 and 2922 cm^{-1} are mainly related to hydroxyl groups; the absorption bands at 2290 and 2067 cm^{-1} are connected to hydrogen bonds due to the presence of oxygen; the absorption bands at 1742 and 1632 cm^{-1} are related to C=O bonds; the absorption bands at 1371 cm^{-1} are related

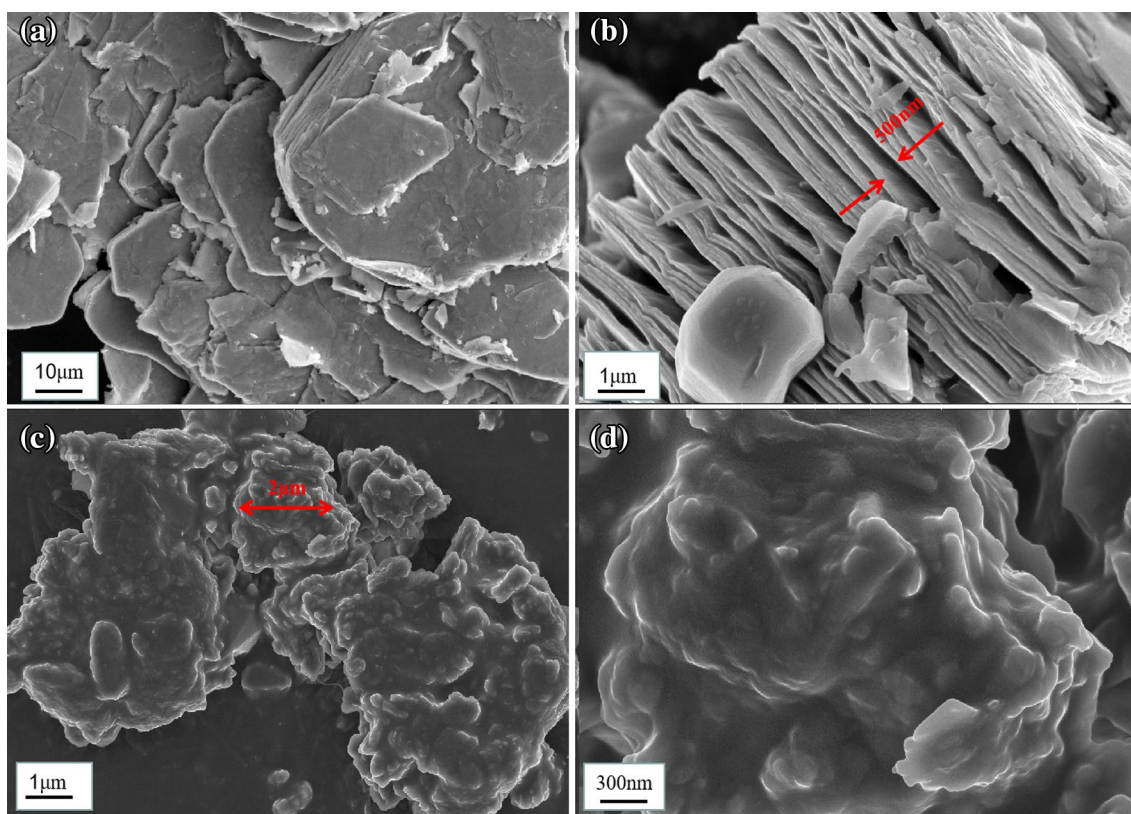**Fig. 3** **a** MXene dispersion **b** MXene powder after corrosion **c** and **d** MXene/EPDM
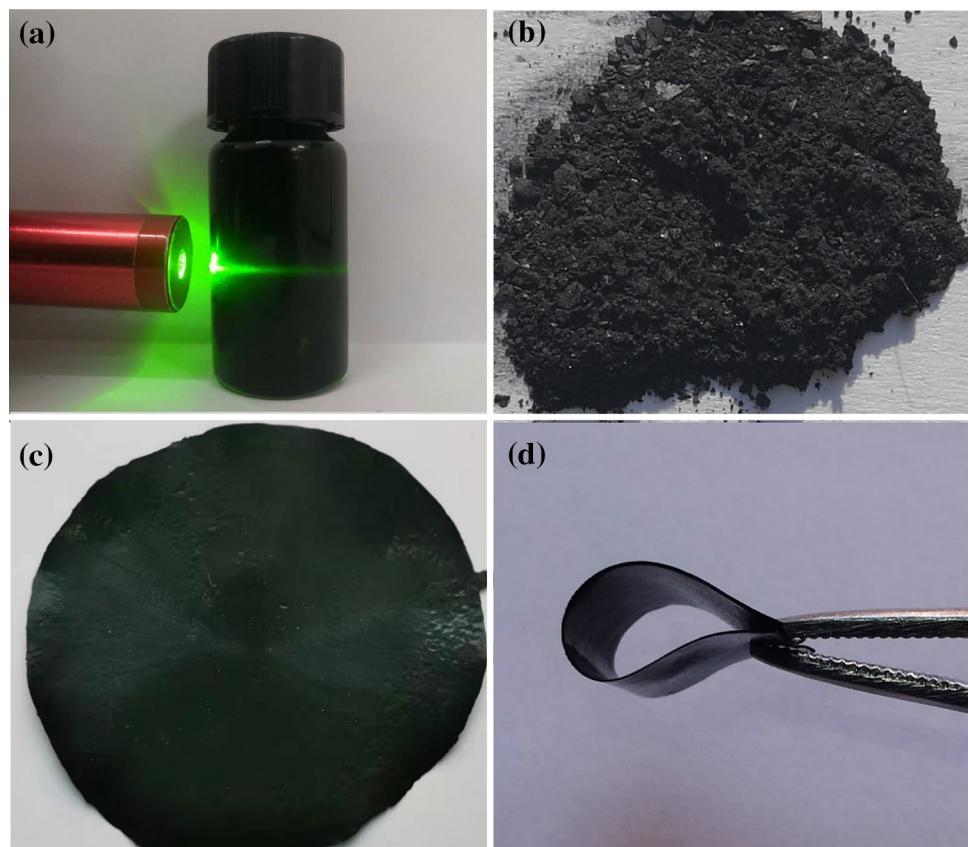
Fig. 4 **a** SEM plane images of MXene, **b** SEM cross-sectional images of MXene and **c** and **d** SEM images of MXene/EPDM Composites
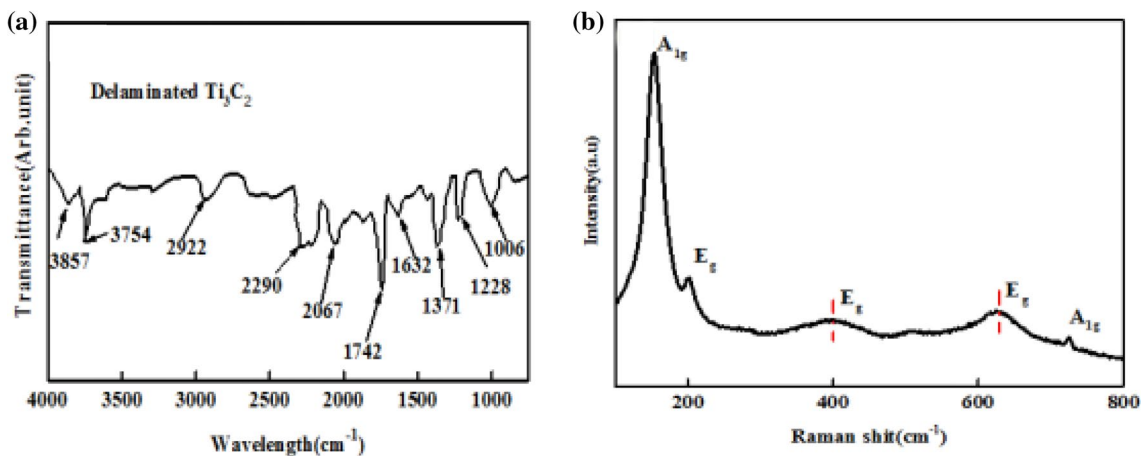

Fig. 5 **a** FTIR spectrum of the delaminated MXene. **b** Raman spectra of MXene

to hydrogen bonds because of the presence of molecular water (O–H); and the energy bands at 1228 and 1006 cm^{-1} correspond to oxygen group vibrations. The FTIR result shows that the main functional groups on the surface of MXene are oxygen and hydroxyl. The F-terminated surfaces of MXene etched in LiF-HCl solution are less than that etched in HF solution. Due to the low concentration of fluorine, there are no peaks or strong peaks associated with the existence of F in the FTIR results. The surface of MXene prepared by this method contains a lot of oxygen and hydroxyl, which enhances its hydrophilicity and makes the sensor to have high sensing performance.

As shown in Fig. 5b, the Raman spectrogram shows the absorption band at 154 cm^{-1}, which is related to the out-of-plane vibration of Ti atom; the band at 725 cm^{-1} is connected to the out-of-plane vibration of C atom, and the peaks

at 202, 392 and 630 cm^{-1} are designated as the in-plane (shear) mode of Ti and C and the surface functional group atoms. The Raman peaks in the MXene phase correspond to Ti–Al and Ti–C peaks. The rise in the peaks of 150-200 cm^{-1} and 300-400 cm^{-1} is due to the introduction of an interlayer adsorbent during the etching process. In addition, the peak at 650 cm^{-1} is due to the stretching of sp^3 carbon. Through Raman spectroscopy, the group structure of MXene can be clearly identified and the structural changes can be analyzed.

3.2 The formula design of MXene/methylbenzene

We control the scale and dispersion of MXene in toluene solution by optimizing the concentration and ultrasonic time. The morphology of MXene/toluene dispersion was characterized by polarizing microscope. Figure 6a, b and c shows the dispersion of MXene in toluene solution at different ultrasonic time, and Mxene cannot be completely dispersed after ultrasound for 15 min. With the increase in ultrasonic time, MXene could be completely dispersed with 90 min ultrasonic time, excessive ultrasonic dispersion can lead to structural damage of MXene, and 90 min can be considered the optimal spread time. Figure 6d, e and f shows the dispersion of MXene in toluene solution at different concentrations. When the concentration of MXene reaches 5%, the distance between MXenes in the dispersion is about 500 nm, and the increase in MXene concentration

reduces the distance between MXenes. However, the high concentration of the dispersion makes MXene agglomerate and difficulty to disperse, the dispersion reaches saturation, and part of Mxene will gather at the content of 15 wt% MXene. In this experiment, 10 wt% MXene toluene dispersion ultrasonic for 90 min was used to prepare MXene/EPDM composite and the distance between MXenes in the dispersion is about 50 nm.

3.3 The conductivity of MXene/EPDM composite

Figure 7a shows that the initial surface resistance of the nanocomposite is about 0.46 kΩ when the distance between two probes is one centimeter. The surface resistance mainly depends on the structure and composition of the dielectric. EPDM rubber shows huge resistance and hardly conductivity, and MXene exhibits excellent conductivity. As a conductive reinforcing material, MXene was dispersed in rubber, which can greatly reduce the surface resistance of rubber and make the surface resistance of rubber reach several hundred ohms or even lower. Figure 7b exhibits that the conductivity of Mxene film measured by the four-probe method about 106.6 S/m. The conductive network formed by MXene sheets enables the film to obtain relatively low resistance and high conductivity.

The conductivity of the MXene films with different mass fractions is shown in Fig. 8a. The electrical conductivity increases from 0.0732 to 106.6 S/m by orders of magnitude
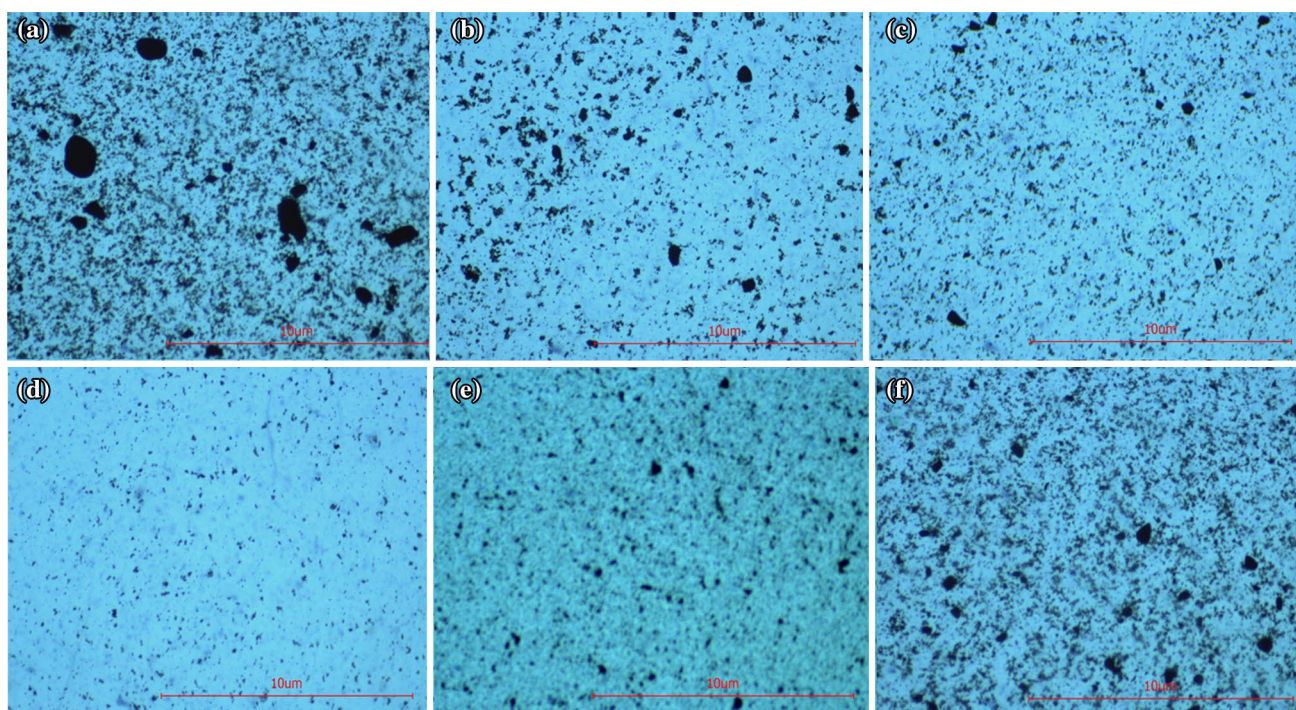

Fig. 6 Dispersions of MXene in toluene **a** sonication 15 min, **b** 45 min and **c** 90 min, **d** Content of MXene in toluene 5%, **e** 10% and **f** 15%

Fig. 7 Conductive performance of the MXene/EPDM film. **a** Initial resistance and **b** the conductivity
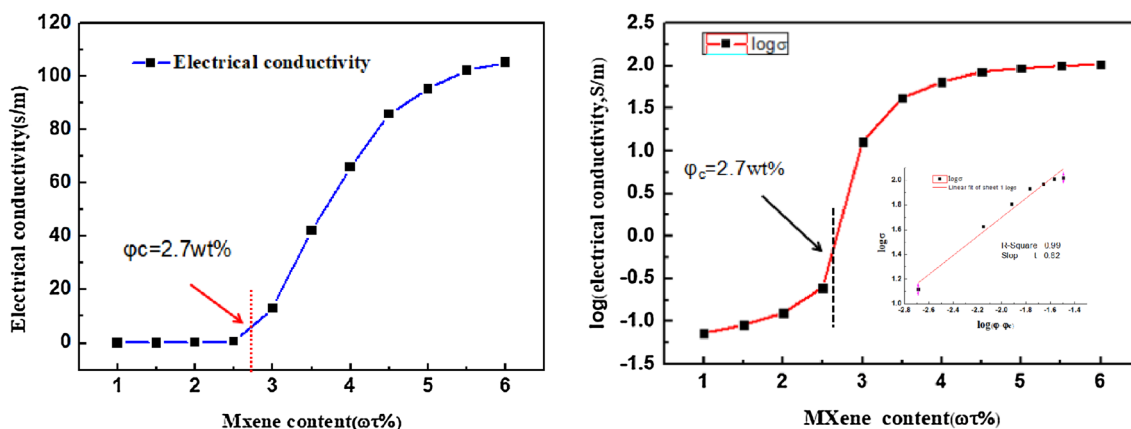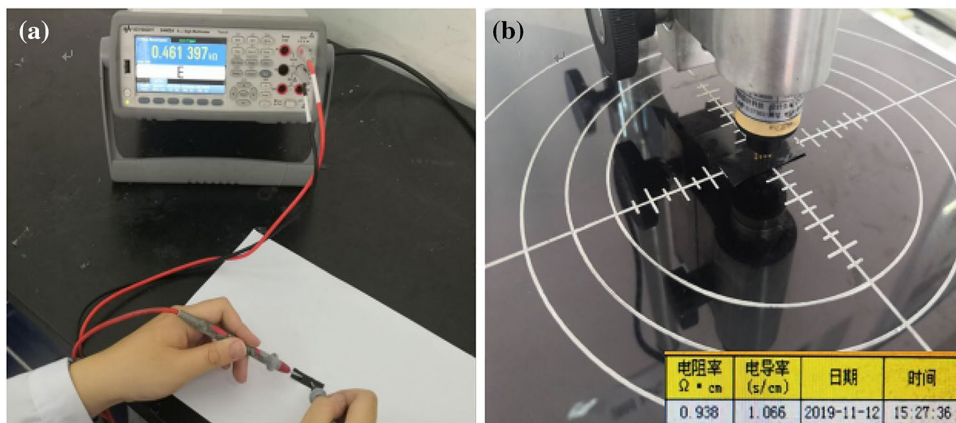

Fig. 8 Electrical conductivity of MXene/EPDM mixture films

with the MXene concentration increasing from 1 to 6%. When the content of MXene is set as low concentration (0 wt% ~ 2.7 wt%), the percolating network is not completely formed and the conductivity changes slightly, while set as 2.7–5 wt%, the electrical conductivity increases substantially due to the formation of percolating network (i.e., the percolation behavior) [34]. And MXene concentration is set as high levels concentration (> 5 wt%), the addition of MXene does not cause sudden changes in electrical conductivity, and the change of electrical conductivity tends to be stable. Because the change of electrical conductivity is smooth after the content of 6% MXene, therefore, we discuss the conductivity of 1–6% in this experiment.

Based on classical percolation theory, the conductivity of MXene/EDPM mixture can be described by Eq. (5) [35].

$$\sigma = \sigma_0(\varphi - \varphi_c)^t \tag{5}$$

where σ is the electrical conductivity of the composite, σ_0 and t are constants, φ is the filler content and φ_c is the percolation threshold. The experimental data are classified

into the legal record $\log \sigma \propto \log (\varphi - \varphi_c)$, and the fitting line will be determined by changing the value of φ_c [36]. The fitting degree reaches the maximum, which is the percolation threshold point. According to the classical percolation threshold theory, the conductive network is not formed completely with the lower MXene content, and the piezoresistive effect exists mainly. However, exceeding the percolation threshold, conductivity increases significantly due to the overlap or tunneling effect of MXene.

As can be seen from Fig. 8b, the log curve of conductivity reflects the change rate of material conductivity. The largest growth range of the change rate from 2 to 3 wt% is about two orders of magnitude. We can draw the percolation threshold in the range of 2–3 wt%, and there is a point in this range where φ_c is the percolation threshold, where the fitting degree of $\log \sigma$ and $\log(\varphi - \varphi_c)$ reaches the maximum. The inset of Fig. 8b is the fitting curve of the percolation threshold. The value of percolation threshold is 2.7%, and the determination coefficient is 99%. This composite has lower percolation threshold and higher electrical conductivity than that of other rubber composites
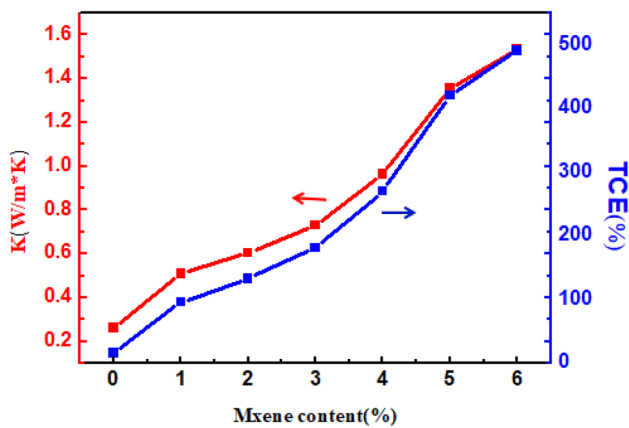
Fig. 9 Thermal conductivity and thermal conductivity enhancement (TCE) of MXene/EDPM composite as a function of EPDM content

(the percolation threshold of (EPDM)@ABS composites reinforced with graphene nanoplatelets (GN) reaches up to 6.6 wt%; the electrical conductivity of natural rubber–graphene is 0.1S/m) [37, 38].

3.4 The thermal conductivity of MXene/EPDM composite

The thermal properties of composites are also important indicators [39]. Figure 9 shows the thermal conductivity (k) as a function of the MXene content. The thermal conductivity of the composite (1 wt%) about 0.5 W/m K is higher than the pure EPDM rubber (0.26 W/m K), it also can be seen that all MXene/EPDM composites exhibit much higher thermal conductivity than pure EPDM rubber, and the thermal conductivity increases in steps with the increase of MXene. Compared with pure EPDM rubber, the thermal conductivity of composite EPDM rubber with 6% MXene content increased from 0.26 to 1.57 W/m K, nearly five times higher. In addition, as shown in Fig. 10, the MXene/EPDM composites also exhibit greater thermal conductivity than 1.96 wt% MXene/SBR, 27.6 vol%BN/SiC, Polyester/graphene, 5 wt%GO/SR, Gnps/PDMS and 8 wt%Gnps/EPDM [40–45]; the reason for heat dissipation performance is that the increase in interaction between MXenes causes the system to form more thermal chains. The improved thermal conductivity of MXene/EPDM mainly attributed to the excellent thermal conductivity of MXene and the formation of a thermal network, but in no case exceeds the thermal conductivity of individual MXene sheets because of the poor thermal conductivity of EPDM.

The thermal conductivity of MXene can be characterized by the thermal conductivity enhancement (TCE) and expressed by the following formulas.
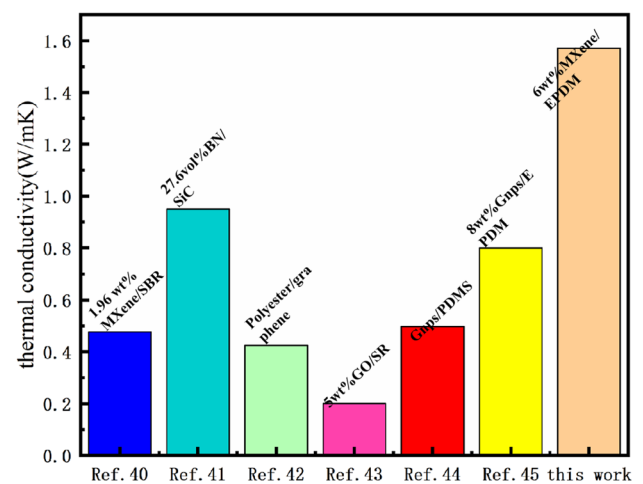

Fig. 10 Comparison of thermal conductivity value of MXene/EPDM composite with previously reported literature values

$$\mathrm{TCE} = \left(\frac{k - k_m}{k_m} \right) \times 100 \tag{6}$$

where K is the thermal conductivity of composites and k_m is the thermal conductivity of the composite matrix. The thermal conductivity growth rate can reflect the effect of filler on the heat dissipation performance of matrix. At low filling rate, the thermal conductivity of composites increases slightly due to the fact that fillers cannot contact each other directly and hardly interact at all. As shown in Fig. 9, with the increase of filler, the thermal conductivity increases significantly; however, further increasing fillers will result in a slow increase in the thermal conductivity of composites, because too many fillers will lead to non-uniform dispersion in the matrix, which will affect the thermal conductivity, and full dispersion will allow more connecting channels and lower thermal resistance between components, so heat can be transferred along these channels quickly [46, 47].

3.5 The mechanical of MXene/EPDM composite

For the film materials used in industry, the mechanical properties cannot be ignored. As is shown in Fig. 11, the stress–strain curves show that the flexibility of MXene/EPDM composites is obvious. It is found that the higher filler-loaded composite (6 wt% MXene/EPDM) does not break at 250% strain which can meet the application requirement. The stress–strain relationship in the elastic region is liner, as defined by the Hooke's Law. The MXene/EPDM exhibits the stronger mechanical than pure EPDM rubber. (Tensile strength increases from 0.85 to 3.06 MPa and elongation at break from 235 to 285%.) The mechanical properties of EPDM rubber with MXene content of 2% will not increase significantly, and tensile strength is 1 MPa, and
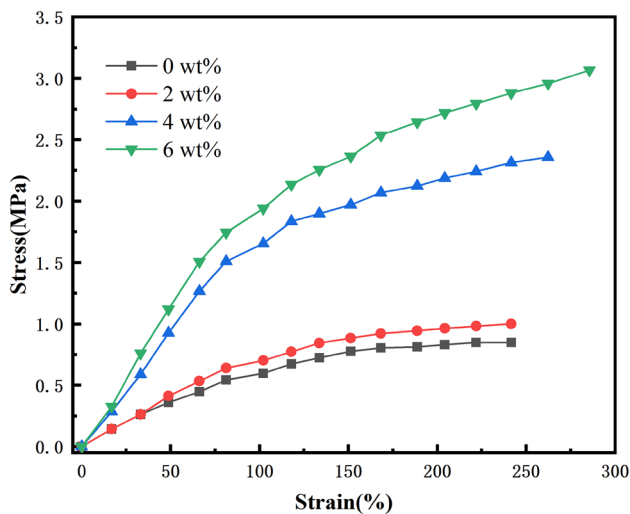
Fig. 11 Tensile stress–strain curves of MXene/EPDM

the Mxene content reaches a high level, and the mechanical properties of the composite are significantly increased. The reasons for the improvement in mechanical properties are as follows:

The excellent mechanical performance of MXene/EPDM is attributed to MXene structure (the addition of Ti_3C_2 nanosheets into the polymer matrix can provide more interfacial interaction, and mechanical performance improved significantly) [48]. When an external force is applied to the composite, the relative slippage in position between the MXene sheets will occur, and a force will be exerted between the interfaces to prevent rubber deformation. Besides, the sufficient dispersion of MXene in rubber increases the transfer of stress in rubber, and the sufficient dispersion of MXene also can be used as a stress transfer center to change the interaction between MXene and EPDM and improve mechanical properties [49]. In summary, the multilayer structure of MXene is conducive to increasing the contact area between layers, the contact force between layers and the stress transfer efficiency.

3.6 Electromagnetic interference(EMI) shielding performance

The SET images of MXene/EPDM with different contents in the range of 8.2–18 GHz (X- and Ku-bands) are shown in Fig. 12a and b, the electromagnetic shielding performance of EPDM is about 7 dB, and the shielding performance of MXene/EPDM increases obviously with the content of MXene. The SET value of 3 wt% MXene/EPDM reaches 25 dB in X-band and 26 dB in Ku-band, which can meet the commercial use standard (20 dB). The MXene/EPDM composite with 6 wt% content shows an average effectiveness of 50 dB at 8.2–18 GHz with the thickness of only 0.3 mm.

In summary, compared with other Mxene-based composites (Table 1), such as 50 wt% MXene/PANI (0.6 mm, 23 dB at 8.2–12.4 GHz) [50], 6.71 vol% MXene/NR (0.33 mm, 53.6 dB at 8.2–12.4 GHz) [51]; 20-MXene/SDS (1.5 mm, 28.5–50.5 dB at 8.2–50.5 GHz) [52], MXene(1000 s/m)/PPY (0.45 mm, 42 dB at 8.2-12.4 GHz) [53], 50 wt% MXene/TOCNF (0.038 mm, 39.6 dB at 8.2–12.4 GHz) [54] and 5 wt% MXene/Epoxy (2 mm, 41 dB at 8.2–12.4 GHz) [55], the new Mxene-based composites in EMI shielding applications have a low content and a comparable shielding performance. In EMI shielding mechanism, shielding efficiency is mainly affected by conductivity and polarization. On the one hand, with the increase in MXene content, MXene conductor circuit path is formed, for composite materials, MXene has higher mobility charge carrying density (electrons or holes) which makes MXene to have a high conductivity and thus can improve dielectric loss and increase shielding effect. On the other hand, MXene has a laminated structure, which increases the interface contact area between MXene and EPDM. The interface and defect of the connection can induce polarization, and multiple refraction and reflection occur when electromagnetic waves enter materials, resulting in weakening of EMI performance. In addition, the thickness of the material also affects the shielding effectiveness. For instance, the shielding efficiency of 10 phr MWCNT/SBR composite is about 35 dB with the thickness of 0.3 mm [45], while at the same thickness, 6 wt% MXene/EPDM exhibits higher shielding efficiency(50 dB) and wider bandwidth.

To further explore the electromagnetic shielding mechanism, we continue to analyze SEA and SER in Fig. 12c and d, and it is observed that SET, SEA and SER of 6% MXene/EPDM at X-band are 47.4 dB, 38.93 dB and 8.47 dB. As can be seen from Fig. 12c and d, SEA(82.1%) plays an important role in the electromagnetic shielding effect, and with the increase in MXene content, the reflection effect is more obvious, and the reflection efficiency is almost unaffected by the frequency. It means that the prepared MXene/EPDM composite is an effective absorbing electromagnetic shielding material.

4 Conclusion

The conclusions are as follows: (1) MXene/EPDM was prepared by a cost-effective method, which combines mechanical blending with solution blending and disperses by ultrasound. (2) When the concentration of MXene toluene dispersion is 10 wt% and 90 min ultrasonic time, the uniform dispersion can be obtained, and the spacing of MXene is about 50 nm. (3) According to the theoretical model, the intrinsic piezoresistive effect and complex internal structure restrict the conductivity below the percolation threshold. With the increase of filler, exceeding the percolation
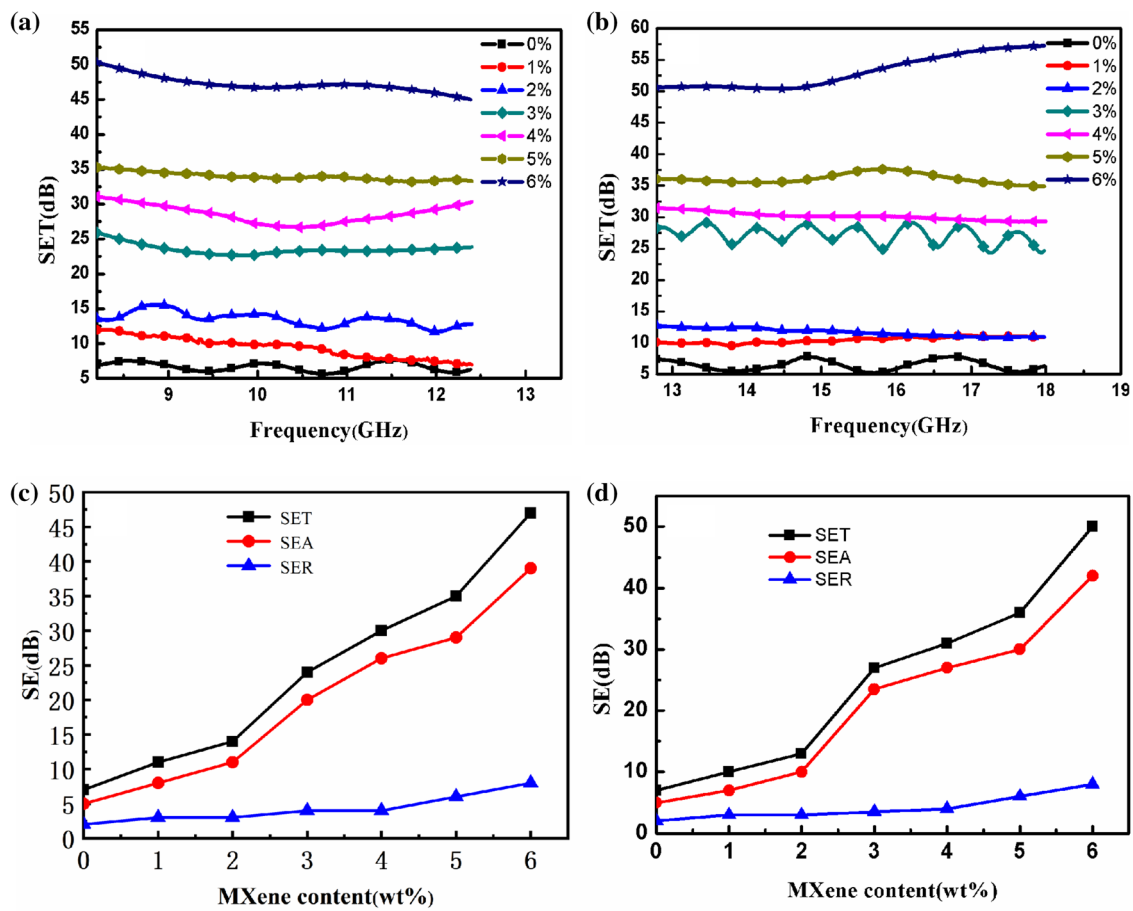
Fig. 12 SET of MXene/EPDM in the X- and Ku-band (**a**) and (**b**) the average SEA, SER and SET of MXene/EPDM in the X- and Ku-band (**c**) and (**d**)

Table 1 Comparison of the reported materials and their corresponding performance

Matrix	Filler	Thickness (mm)	SET (dB)	Shielding frequency	References
PANI	50 wt% MXene	0.6	23	8.2–12.4	[50]
NR	6.71 vol% MXene	0.33	53.6	8.2–12.4	[51]
SDS	20-MXene/CNT	1.5	28.5–50.5	8.2–12.4	[52]
PPY	1000 s/m MXene	0.45	42	8.2–12.4	[53]
TOCNF	50 wt%MXene	0.038	39.6	8.2–12.4	[54]
Epoxy	5 wt% MXene	2	41	8.2–12.4	[55]
EPDM	6 wt% MXene	0.3	50	8.2–18	This work

threshold, the overlap of MXene and the tunneling effect increase the flow of electronic load, which increases the conductivity. (4) MXene/EPDM composites were prepared by grading dissolution and optimization of ultrasonic power and time. The composites have a low percolation threshold of 2.7 wt% and a high conductivity of 106.6 S/m at 6 wt%. (5) At MXenes loading of 6 wt%, the thermal conductivity increases to 1.57 W/m K. The structure of thermal conductivity significantly improves the reliability of the material and reduces the heat generated by the material in harsh environment. (6) The absorption-dominated SET of 6 wt% MXene/EPDM reaches 50 dB in X-band (8.2–12.4 GHz) and 52 dB in Ku-band (12.4–18 GHz), with a thickness of only 0.3 mm. The MXene critical load required for composites meeting commercial EMI shielding applications (20 dB) with only 3 wt%. MXene/EPDM can be regarded as an ideal shielding material for EMI. (7) MXene/EPDM has excellent thermal conductivity, electrical conductivity and electromagnetic effect. It can be used in the next generation of flexible electronic products by simple and sustainable

methods. We believe that MXene/EPDM will provide new ways for applications in next-generation commercial portable flexible electrons.

Reference

1. B. Hao et al., Lightweight graphite membranes with excellent electromagnetic interference shielding effectiveness andcr thermal conductivity. J. Mater. Sci.: Mater. Electron. **30**(7), 6734–6744 (2019)

2. P. Kumar, A. Kumar, K.Y. Cho et al., An asymmetric electrically conducting self-aligned graphene/polymer composite thin film for efficient electromagnetic interference shielding[J]. AIP Adv. **7**(1), 015103 (2017)

3. B. Shen, W. Zhai, W. Zheng, Ultrathin flexible graphene film: an excellent thermal conducting material with efficient EMI shielding[J]. Adv. Func. Mater. **24**(28), 4542–4548 (2014)

4. R. Xiaohu, C. Yankui, Electromagnetic and microwave absorbing properties of carbonyl iron/BaTiO_3 composite absorber for matched load of isolator[J]. J. Magn. Magn. Mater. **393**, 293–296 (2015)

5. S.P. Gairola et al., Retracted: EMI shielding effectiveness of expanded graphite and reduced graphene oxide. J. Chin. Chem. Soc. **66**(7), 785 (2019)

6. Y. Li, B. Shen, X.L. Pei, Y.G. Zhang, D. Yi, W.T. Zhai, L.H. Zhang, X.C. Wei, W.G. Zheng, Ultrathin carbon foams for effective electromagnetic interference shielding. Carbon **100**, 375–385 (2016)

7. S. Maiti, S. Suin, N.K. Shrivastava et al., A strategy to achieve high electromagnetic interference shielding and ultra low percolation in multiwall carbon nanotube–polycarbonate composites through selective localization of carbon nanotubes[J]. Rsc. Adv. **4**(16), 7979 (2014)

8. Z. Ning et al., Flexible and transparent graphene/silver-nanowires composite ?lm for high electromagnetic interference shielding effectiveness. Sci. Bull. **4**(30), 540–546 (2019)

9. D. Jasvir et al., EMI shielding properties of laminated graphene and PbTiO 3 reinforced poly(3,4-ethylenedioxythiophene) nanocomposites. Compos. Sci. Technol. **165**, 222–230 (2018)

10. H. Furong, W. Yimeng, W. Peiyu et al., Oxidized multiwall carbon nanotube/silicone foam composites with effective electromagnetic interference shielding and high gamma radiation stability[J]. Rsc. Adv. **8**(43), 24236–24242 (2018)

11. F. Ren, D. Song, Z. Li et al., Synergistic effect of graphene nanosheets and carbonyl iron–nickel alloy hybrid filler on electromagnetic interference shielding and thermal conductivity of cyanate ester composites[J]. J. Mater. Chem. C **6**, 1476–1486 (2018)

12. S. Lu et al., Highly stretchable and sensitive sensor based on GnPs/EPDM composites with excellent heat dissipation performance. Appl. Phys. A **125**(6), 425 (2019)

13. Y. Liu et al., Graphene enhanced flexible expanded graphite film with high electric, thermal conductivities and EMI shielding at low content. Carbon **135**, 435–445 (2018)

14. P. Zhang et al., Fabrication of novel MXene (Ti3C2)/polyacrylamide nanocomposite hydrogels with enhanced mechanical and drug release properties. Soft Matter **16**(1), 162–169 (2020)

15. Z. Wang et al., Recent advances on metal-free graphene-based catalysts for the production of industrial chemicals. Front. Chem. Eng. China **12**(4), 855–866 (2018)

16. M. Ahmadi et al., 2D transition metal dichalcogenide nanomaterials: advances, opportunities, and challenges in multi-functional polymer nanocomposites. J. Mater. Chem. **8**(3), 845–883 (2020)

17. G. Xu et al., Solvent-regulated preparation of well-intercalated Ti_3C_2Tx MXene nanosheets and application for highly effective electromagnetic wave absorption. Nanotechnology **29**(35), 355201 (2018)

18. T. Li et al., A flexible pressure sensor based on an MXene–textile network structure. J. Mater. Chem. C **7**(4), 1022–1027 (2019)

19. M. Naguib, V.N. Mochalin, M.W. Barsoum et al., 25th anniversary article: mxenes: a new family of two-dimensional materials[J]. Adv. Mater. **26**(7), 992–1005 (2014)

20. X. Zhan et al., MXene and MXene-based composites: synthesis, properties and environment-related applications. Nanoscale Horiz. **5**, 235–258 (2020)

21. J. Halim et al., X-ray photoelectron spectroscopy of select multilayered transition metal carbides (MXenes). Appl. Surf. Sci. **362**, 406–417 (2016)

22. A. Mishra et al., Isolation of pristine MXene from Nb4AlC3 MAX phase: a first-principles study. Phys. Chem. Chem. Phys. **18**(16), 11073–11080 (2016)

23. S. Ankita et al., MXene: an emerging material for sensing and biosensing. TrAC Trends Anal. Chem. **105**, 424–435 (2018)

24. Q. Jiang, All pseudocapacitive MXene-RuO_2 asymmetric supercapacitors. Adv. Energy Mater. **8**(13), 1703043 (2018)

25. Y. Liu et al., Excellent catalytic activity of a two-dimensional Nb4C3Tx (MXENE) on hydrogen storage of MgH2. Appl. Surf. Sci. **493**, 431–440 (2019)

26. H. Wu, L.T. Drzal, Graphene nanoplatelet paper as a light-weight composite with excellent electrical and thermal conductivity and good gas barrier properties[J]. Carbon **50**(3), 1135–1145 (2012)

27. Y. Qing, W. Zhou, F. Luo et al., Titanium carbide (MXene) nanosheets as promising microwave absorbers[J]. Ceram. Int. **42**(14), 16412–16416 (2016)

28. Y.J. Wan, P.L. Zhu, S.H. Yu et al., Graphene paper for exceptional EMI shielding performance using large-sized graphene oxide sheets and doping strategy[J]. Carbon **122**, 74–81 (2017)

29. T. Tomaegovi et al., Effect of the common solvents on UV-modified photopolymer and EPDM flexographic printing plates and printed ink films. Coatings **10**(2), 136 (2020)

30. S. Azizi et al., Electrical and thermal phenomena in low-density polyethylene/carbon black composites near the percolation threshold. J. Appl. Polym. Sci. **136**(6), 47043 (2019)

31. Reduced Graphene Oxides, Light-weight and high-efficiency electromagnetic interference shielding at elevated temperatures[J]. Adv. Mater. **26**(21), 3484–3489 (2014)

32. Y.B. Pottathara, V. Bobnar, S. Gorgieva et al., Mechanically strong, flexible and thermally stable graphene oxide/nanocellulosic films with enhanced dielectric properties[J]. RSC Adv. **6**(54), 49138–49149 (2016)

33. Zhang et al., Preparation and characterization of graphene paper for electromagnetic interference shielding[J]. Carbon **82**(30), 353–359 (2015)

34. A. Chatterjee et al., Heat conduction model based on percolation theory for thermal conductivity of composites with high volume fraction of filler in base matrix. Int. J. Thermal Sci. **136**, 389–395 (2019)

35. B. Rezaei et al., High conductive ITO-free flexible electrode based on Gr-grafted-CNT/Au NPs for optoelectronic applications. Opt. Mater. **89**, 441–451 (2019)

36. K. Gnanasekaran et al., A unified view on nanoscale packing, connectivity, and conductivity of CNT networks. Adv. Funct. Mater. **29**(13), 1807901 (2019)

37. F. Wang, Y. Zhang, B.B. Zhang et al., Enhanced electrical conductivity and mechanical properties of ABS/EPDM composites filled with graphene[J]. Compos. Part B Eng. **83**, 66–74 (2015)

38. C.S. Boland, U. Khan, C. Backes et al., Sensitive, high-strain, high-rate bodily motion sensors based on graphene-rubber composites[J]. ACS Nano **8**(9), 8819–8830 (2014)

39. A. Bu et al., Plasma electrolysis spraying Al_2O_3 coating onto quartz fiber fabric for enhanced thermal conductivity and stability. Appl. Ences **10**(2), 702 (2020)

40. Q. Li et al., Ti_3C_2 MXene as a new nanofiller for robust and conductive elastomer composites. Nanoscale **11**(31), 14712–14719 (2019)

41. Y. Yang et al., Thermal conductivity and mechanical properties of polyimide composites with mixed fillers of BN flakes and SiC @SiO2 whiskers. Polym. Eng. Ence **5**, 1044–1053 (2020)

42. G. Manasoglu et al., Electrical resistivity and thermal conductivity properties of graphene↘oated woven fabrics. J. Appl. Polym. Ence **11**, 48024 (2019)

43. P. Liu, X. Zhang, H. Jia et al., High mechanical properties, thermal conductivity and solvent resistance in graphene oxide/styrene-butadiene rubber nanocomposites by engineering carboxylated acrylonitrile-butadiene rubber[J]. Compos. Part B Eng. **130**, 257–266 (2017)

44. C. Shen et al., Silica coating onto graphene for improving thermal conductivity and electrical insulation of graphene/polydimethylsiloxane nanocomposites. J. Mater. Sci. Technol. **35**(1), 36–43 (2019)

45. S. Lu et al., Flexible GnPs/EPDM with excellent thermal conductivity and electromagnetic interference shielding properties. NANO **14**(06), 1950075 (2019)

46. F. Lv et al., High cross-plane thermally conductive hierarchical composite using graphene-coated vertically aligned carbon nanotubes/graphite. Carbon **149**, 281–289 (2019)

47. Q. Zhang, J. Liu, Anisotropic thermal conductivity and photodriven phase change composite based on RT100 infiltrated carbon nanotube array. Solar Energy Mater Solar Cells **190**, 1–5 (2019)

48. L.C. Jia, Y.K. Li, D.X. Yan, Flexible and efficient electromagnetic interference shielding materials fromground tirerubber[J]. Carbon **121**, 267–273 (2017)

49. N. Joseph, C. Janardhanan, M.T. Sebastian, Electromagnetic interference shielding properties of butyl rubber-single walled carbon nanotube composites[J]. Compos. Sci. Technol. **101**, 139–144 (2014)

50. S. Kumar, K.P. Arti et al., Steady microwave absorption behavior of two-dimensional metal carbide MXene and Polyaniline composite in X-band[J]. J. Magn. Magn. Mater. **488**, 165364 (2019)

51. L. Jia-Qi, Z. Sai, Z. Hao-Bin, Z. Deng, L. Li, Yu. Zhong-Zhen, Flexible, stretchable and electrically conductive MXene/natural rubber nanocomposite films for efficient electromagnetic interference shielding[J]. Compos. Sci. Technol. **182**, 107754 (2019)

52. K. Raagulan, R. Braveenth, L. Ro Lee et al., Fabrication of flexible, lightweight, magnetic mushroom gills and coral-like mxene–carbon nanotube nanocomposites for EMI shielding application[J]. Nanomaterials **9**(4), 519 (2019)

53. Q.W. Wang, H.B. Zhang, J. Liu et al., Multifunctional and water-resistant mxene-decorated polyester textiles with outstanding electromagnetic interference shielding and joule heating performances[J]. Adv. Funct. Mater. **29**(7), 1806819 (2019)

54. Z. Zhan et al., Ultrastrong and conductive MXene/cellulose nanofiber films enhanced by hierarchical nano-architecture and interfacial interaction for flexible electromagnetic interference shielding. J. Mater. Chem. C **7**(32), 9820–9829 (2019)

55. W. Lei et al., Fabrication on the annealed Ti_3C_2Tx MXene/ Epoxy nanocomposites for electromagnetic interference shielding application[J]. Compos. Part B Eng. **171**, 111–118 (2019)